Electron-Nucleus Hyperfine Coupling Calculated from Restricted Active Space Wavefunctions and an Exact Two-Component Hamiltonian

Rulin Feng, Thomas J. Duignan and Jochen Autschbach*

Department of Chemistry
University at Buffalo
State University of New York
Buffalo, NY 14260-3000, USA
email: jochena@buffalo.edu

Abstract: Exact two-component (X2C) relativistic nuclear hyperfine magnetic field operators were incorporated in X2C ab-initio wavefunction calculations at the multi-reference restricted active space (RAS) level for calculations of nuclear hyperfine magnetic properties. Spin-orbit coupling was treated via RAS state interaction (SO-RASSI). The method was tested by calculations of electron – nucleus hyperfine coupling constants. The approach, implemented in the OpenMolcas program, overcomes a major limitation of a previous SO-RASSI implementation for hyperfine coupling that relied on non-relativistic hyperfine operators [J. Chem. Theor. Comput. 2015, 11, 538–549] and therefore had only limited applicability. Results from calculations on systems with light and heavy main group elements, transition metals, lanthanides, and one actinide complex, demonstrate reasonably good agreement with experimental data, where available, as long as the active space can generate sufficient spin polarization.

1 Introduction

Electron paramagnetic resonance (EPR) is a magnetic resonance spectroscopic technique used to probe atomic and molecular species with unpaired electrons. The electron-nucleus hyperfine coupling (HFC), which arises from the interaction between the spin magnetic moments of a given nucleus and the electrons, is essential to understanding the peak splittings of an EPR experimental spectrum. HFC in itself contains a wealth of information about the distribution of the magnetization in a molecule, or details about the electronic structure at an open-shell metal center in a complex. The EPR spectra are analyzed using a pseudospin Hamiltonian. The HFC tensor and the associated HFC constants (HFCC)[1–3] are obtained, along with the other parameters in the pseudospin Hamiltonian, from fitting the eigenvalues of the Hamiltonian to the measured spectrum.

Computational predictions for the the HFCCs from quantum chemical methods are important for gaining insight about structure and bonding from the measurements.[4,5] Hereby a reliable *ab initio* electronic structure underlies the calculation of HFC, and this generally means a high-level relativistic electron correlation method is required, along with a proper relativistic treatment of the hyperfine operator in an atomic orbital (AO) basis.

The development of theoretical methods for calculating HFC and other hyperfine interactions, such as nuclear magnetic shielding and indirect nuclear spin-spin coupling, has remained an active field of research for many decades. In single-reference methods such as Hartree-Fock (HF) and Kohn-Sham (KS) theory, HFC calculations require a spin unrestricted approach to generate the all-important spin polarization. By design, this approach introduces spin contamination, which may lead to inaccurate results.[6–8] In wavefunction calculations, the effects of electron correlation on HFC have been treated with many-body perturbation theory (MBPT), coupled-cluster (CC) theory, and configuration interaction (CI).[7,9–21] The CC methods typically provide the most accurate results, but they are either limited to single-reference wavefunctions or limited to relatively small systems. MBPT methods, especially in lowest (second) order (PT2), are promising, since they can be utilized with both single-reference and multi-reference wavefuntions to efficiently capture dynamic electron correlation. CI and complete active space (CAS) methods are the most straightforward to use for multi-reference calculations on open-shell systems, but short of full CI it is difficult to capture the effects of spin polarization and spin delocalization to a degree sufficient to describe HFC, and in particular its Fermi contact contribution (vide infra). Shiozaki and Yanai developed a CASPT2 method for HFC in which most of the spin polarization was generated via the relaxed PT2 spin density matrix.[20] A 'restricted-unrestricted' approach has been described,[15] in which the hyperfine perturbation acts on spin-restricted multi-configurational wavefunctions to generate the desired spin polarization to first order in perturbation theory, but the method is not widely available. Alternatively, it has been suggested to employ density matrix renormaliza-

tion group (DMRG)[22,23] algorithms in CAS calculations to increase the active space for a better description of the spin polarization.[24]

Relativistic effects[25,26] are of crucial importance for systems that contain heavy elements, and in particular for properties that involve the nuclear magnetic hyperfine operators. While there has been great progress in the development of four-component (4c) relativistic methods for the calculation of magnetic properties,[27–32] an existing nonrelativistic quantum chemistry program code is likely more easily retrofitted for a two-component (2c) relativistic Hamiltonian, and there are good reasons for adopting a 2c framework also for a new code. The variationally stable zeroth-order regular approximation (ZORA)[33] and low-order Douglas-Kroll-Hess (DKH)[34] approximate 2c (quasirelativistic) Hamiltonians have been used for a long time for relativistic magnetic property calculations.[26,35] It is fair to state that the treatment of magnetic properties such as HFC within ZORA[36–38] is comparatively easy, compared to DKH beyond first order,[39,40] apart from general issues such as the dependence of magnetic properties on the gauge origin chosen for the vector potential in finite-basis set calculations. (For properties that only depend on nuclear hyperfine magnetic moments, such as HFC or the indirect nuclear spin-spin coupling, field dependent basis sets are typically not used because the gauge origin is naturally defined at the position of the nucleus.) Magnetic properties were eventually calculated with DKH to arbitrary order,[41,42] offering access to fully relativistic results from 2c calculations. However, in the meantime 'exact two-component' (X2C) methods have emerged, where matrix representations of the 2c (one-electron) Hamiltonian in a basis are constructed directly along with the transformation matrices from the 4c to the 2c picture.[43–46] The treatment of the electron correlation and quantum electrodynamic (QED) effects remains a challenge,[47,48] but X2C has opened the way to determine the matrix representations for fully relativistic 2c one-electron operators, i.e., capturing all picture-change effects, needed for molecular property calculations, including magnetic properties.[49–57]

Our group has previously devised an approach for HFC calculations[19] within the restricted active space (RAS) self-consistent field (RASSCF)[58–61] and RAS-CI wavefunction frameworks, with inclusion of the spin-orbit (SO) coupling (SOC) via state interaction (RASSI) .[62,63] Spin-free wavefunctions included scalar relativistic effects at the second-order DKH level (DKH2), and the SOC interaction was determined with DKH-based atomic mean-field integrals (AMFI).[64–66] The approach was formulated for Kramers doublets, following an analogous scheme for EPR g-tensors.[67] The RAS partitioning provided a way to generate important contributions to the spin polarization via single excitations among a large number of orbitals, in addition to the principal active space used to describe the open shells. Although this route toward the spin polarization has its limitations, it was found suitable also for describing Curie-paramagnetic contributions to NMR shifts,[68] which are closely related to HFC.[69,70] As implemented, the HFC calculations had a major drawback in that the underlying nuclear magnetic hyperfine operators were non-relativistic.

Accordingly, applications were limited to light atomic systems, the HFC of light ligand atoms in heavy metal complexes, or the HFC of heavy metal centers with negligible Fermi contact contributions (e.g., an unpaired electron in an f shell). As an example for the latter, it was shown that the HFC of ^{237}Np in NpF_6 agreed very well with experimental data. The same approach, effectively, was also used by others recently, to calculate HFC parameters of Tb and Dy in lanthanide complexes.[71,72]

The present article is concerned with the generalization of the HFC approach reported in Reference 19 to X2C, based on the X2C transformed nuclear magnetic hyperfine operator as described in Reference 53. The implementation was carried out in OpenMolcas.[73] The construction of the X2C transformed HFC operator, the implementation within the SO-RASSI framework, and other methodological aspects are detailed in Section 2. Section 4 provides the calculations of a collection of molecules to test its validity. A brief conclusion & outlook are given in Section 5.

2 Methodology

Scalars and scalar operators are denoted by italic notation such as h, x. Vectors, and vector operators are represented in bond-italic notation such as $\boldsymbol{r}$, $\boldsymbol{p}$, respectively. Matrices and operator matrix representations in a 2×2 super-matrix structure are indicated by upright-bold notation such as $\mathbf{h}, \mathbf{A}$. The vector of the Pauli spin matrices $\boldsymbol{\sigma}$, and the individual spin matrices are $\boldsymbol{\sigma}_x, \boldsymbol{\sigma}_y, \boldsymbol{\sigma}_z$. For the Dirac picture, the 4×4 block structure of the matrix representation of an operator is indicated by notation such as $\mathbb{U}, \mathbb{h}$.

2.1 X2C Transformation of the Electron-Nucleus Hyperfine Operator

The X2C decoupling transformation applied to magnetic field operators follows a previous publication by one of us.[53] We repeat the key steps to render the article self-contained. Starting from the Dirac one-electron Hamiltonian matrix $\mathbb{h}^0_{\mathrm{D}}$, a unitary transformation generates the matrix representation of a de-coupled two-component operator $\mathbf{h}_{\mathrm{X2C}}$ with an eigenvalue equation in the metric (overlap) $\mathbf{S}$ of the chosen basis set. Specifically,

$$\mathbb{U}^{\dagger}\mathbb{h}^0_{\mathrm{D}}\mathbb{U} = \begin{bmatrix} \mathbf{h}_{\mathrm{X2C}} & \mathbf{0} \\ \mathbf{0} & \cdots \end{bmatrix} \tag{1}$$

with the unitary matrix

$$\mathbb{U} = \begin{bmatrix} \mathbf{U}^{\mathrm{UU}} & \mathbf{U}^{\mathrm{UL}} \\ \mathbf{U}^{\mathrm{LU}} & \mathbf{U}^{\mathrm{LL}} \end{bmatrix} \tag{2}$$

In Equation (2), the superscripts U and L denote 'upper' and 'lower' 2-spinor component (or 'large' and 'small' component) of the Dirac 4-spinor. The $\mathbf{h}_{\mathrm{X2C}}$ is the desired exact two-component one-electron Hamiltonian matrix, $\mathbf{0}$ means a matrix filled with zeros, and $\cdots$ means the block is not of interest in this work. The calculation of of $\mathbf{h}_{\mathrm{X2C}}$ and the transformation matrix is typically based on a matrix representation of Dyall's modified Dirac Equation (mDE).[43,74] The mDE is equivalent to the unmodified Dirac equation if a restricted kinetic balance (RKB)[75–77] basis is adopted for the lower components of the Dirac 4-spinors. That is, when χ_μ is an atomic orbital (AO) basis function for the upper component, and $\{\xi_\mu\}$ is a corresponding basis function for the lower component, the RKB condition is

$$\{\xi_\mu\} = \left\{ \frac{1}{2mc}(\boldsymbol{\sigma}\cdot\boldsymbol{p})\chi_\mu \right\} \tag{3}$$

Here, m and c are the electron rest mass and speed of light, respectively, and $\boldsymbol{p}$ is the linear momentum operator. The RKB condition facilitates the connection between the large and small component of the wavefunction in the absence of a magnetic field. In the presence of a magnetic field, represented by a vector potential $\boldsymbol{A}$, the minimal substitution $\boldsymbol{p} \to \boldsymbol{p} + e\boldsymbol{A}$ is applied, where e is the unit charge. The substitution gives the Dirac Hamiltonian

$$h_{\mathrm{D}} = h_{\mathrm{D}}^{0} + h_{\mathrm{D}}^{\mathrm{mag}} \tag{4}$$

with

$$h_{\mathrm{D}}^{0} = \begin{bmatrix} V & \boldsymbol{\sigma}\cdot\boldsymbol{p} \\ \boldsymbol{\sigma}\cdot\boldsymbol{p} & V - 2mc^2 \end{bmatrix} \quad \text{and} \quad h_{\mathrm{D}}^{\mathrm{mag}} = ec \begin{bmatrix} \mathbf{0} & \boldsymbol{\sigma}\cdot\boldsymbol{A} \\ \boldsymbol{\sigma}\cdot\boldsymbol{A} & \mathbf{0} \end{bmatrix} \tag{5}$$

Here, h_{D}^{0} is the Dirac Hamiltonian in the absence of external fields, with the energy origin shifted to the electron rest mass, and $h_{\mathrm{D}}^{\mathrm{mag}}$ accounts for the presence of a magnetic field. We make the minimal substitution in the Dirac Hamiltonian, but not in the balance condition of Equation (3), so that the basis set is not magnetic field-dependent. In response calculations with magnetic fields, magnetic balance, in addition to kinetic balance, is needed to keep the magnetic-field response of the large and small components balanced.[27,32,78,79] However, first-order magnetic properties such as hyperfine coupling can formally be calculated without invoking the response to a magnetic field, and therefore RKB would seem to be a reasonable approximation in the present calculations. There is also good evidence from numerical data in the literature that the approximations used here are unlikely to introduce large errors. Further details are given at the end of this section.

The vector potential $\boldsymbol{A}$ may have different sources. An external magnetic field is not considered here. The vector potential of interest in this work is the one arising from the magnetic field generated by the spin magnetic moment $\boldsymbol{m}_K$ of a nucleus K located at $\boldsymbol{R}_K$. For a point magnetic

dipole,

$$\boldsymbol{A}(\boldsymbol{r}) = \varkappa \boldsymbol{m}_K \times \frac{\boldsymbol{r}_K}{r_K^3} \tag{6}$$

with $\boldsymbol{r}_K = \boldsymbol{r} - \boldsymbol{R}_K$ and $r_K = |\boldsymbol{r}_K|$. Furthermore, $\varkappa = \mu_0/(4\pi)$ in SI units, μ_0 is the magnetic constant or vacuum permeability. In atomic units, $\varkappa = c^{-2}$. As is customary, the gauge origin for the hyperfine field has been chosen to coincide with the position of the nucleus. The hyperfine field $\boldsymbol{A}$ is in the Coulomb gauge, i.e., $\boldsymbol{\nabla} \cdot \boldsymbol{A} = 0$. The magnetic moment of the nucleus can also be 'smeared out', for example with a spherical Gaussian function, in order to treat finite nuclear volume effects[39,80–82] on the same approximate footing as does a commonly used model for finite nuclear charge distributions.[83,84] However, prior HF and DFT test calculations with X2C in a different program,[53] and numerous reports of calculations of NMR parameters (see, for example, References 55,85) have shown that the combination of finite nuclear volumes for the potential and point magnetic dipoles for the hyperfine interaction is a reasonable approximation.

For first-order properties such as the electron-nucleus hyperfine coupling interaction, the X2C transformation of Equation (1) may be applied directly to the 4-component perturbation operator obtained from Equation (5), if the operator is represented in the RKB basis. For calculations of the hyperfine coupling tensor components, one needs to take the first derivative with respect to the u component ($u \in \{x, y, z\}$) of the nuclear spin magnetic moment vector $\boldsymbol{m}_K$,

$$h_{\mathrm{D}}^{\mathrm{mag},u} = \left.\frac{\partial h_{\mathrm{D}}^{\mathrm{mag}}}{\partial m_{K,u}}\right|_{\boldsymbol{m}_K=0} = ec\varkappa \begin{bmatrix} \mathbf{0} & \left(\frac{\boldsymbol{r}_K}{r_K^3} \times \boldsymbol{\sigma}\right)_u \\ \left(\frac{\boldsymbol{r}_K}{r_K^3} \times \boldsymbol{\sigma}\right)_u & \mathbf{0} \end{bmatrix} \tag{7}$$

where superscript u indicates the derivative, and subscript u the corresponding vector component. The perturbation operator matrix transformation then reads

$$\mathbf{h}_{\mathrm{X2C}}^{\mathrm{mag},u} = \mathbf{U}^{\mathrm{LU}\dagger}\mathbf{h}^{\mathrm{LU},u}\mathbf{U}^{\mathrm{UU}} + \mathbf{U}^{\mathrm{UU}\dagger}\mathbf{h}^{\mathrm{UL},u}\mathbf{U}^{\mathrm{LU}} \tag{8}$$

Here, $\mathbf{h}^{\mathrm{UL},u}$ and $\mathbf{h}^{\mathrm{LU},u}$ are the AO matrix representations of the corresponding components of the operator in Equation (7) in the mixed upper/lower and lower/upper component basis, respectively. The individual matrix elements are

$$h_{\mu\nu}^{\mathrm{UL},u} = \frac{e\varkappa}{2m}\left\langle \chi_\mu \middle| [\frac{\boldsymbol{r}_K}{r_K^3} \times \boldsymbol{\sigma}]_u \middle| (\boldsymbol{\sigma} \cdot \boldsymbol{p})\chi_\nu \right\rangle \tag{9a}$$

$$h_{\mu\nu}^{\mathrm{LU},u} = \frac{e\varkappa}{2m}\left\langle (\boldsymbol{\sigma} \cdot \boldsymbol{p})\chi_\mu \middle| [\frac{\boldsymbol{r}_K}{r_K^3} \times \boldsymbol{\sigma}]_u \middle| \chi_\nu \right\rangle \tag{9b}$$

With $\boldsymbol{p} = -i\hbar\boldsymbol{\nabla}$ and the shorthand notation $\boldsymbol{F} = [\hbar e\varkappa/(2m)]\boldsymbol{r}_K/r_K^3$, after separating the spin-

dependent and spin-independent part of the AO matrix elements, the matrix elements can be written in the following form,

$$h_{\mu\nu}^{\mathrm{UL},u} = -i\mathbf{1}\langle\mu|(\boldsymbol{F}\times\boldsymbol{\nabla})_u|\nu\rangle - \sigma_u\langle\mu|\boldsymbol{F}\cdot\boldsymbol{\nabla}|\nu\rangle + \sum_v \sigma_v\langle\mu|F_v|\partial_u\nu\rangle \tag{10a}$$

$$h_{\mu\nu}^{\mathrm{LU},u} = i\mathbf{1}\langle(\boldsymbol{F}\times\boldsymbol{\nabla})_u\mu|\nu\rangle - \sigma_u\langle\boldsymbol{F}\cdot\boldsymbol{\nabla}\mu|\nu\rangle + \sum_v \sigma_v\langle\partial_u\mu|F_v|\nu\rangle \tag{10b}$$

The 4-component magnetic perturbation operator matrix in the RKB basis can therefore be calculated easily from AO matrices with elements $\langle\mu|F_u|\partial_v\nu\rangle$ for the different combinations of u and v. Subsequently, the desired two-component magnetic perturbation operator matrix $\mathbf{h}_{\mathrm{X2C}}^{\mathrm{mag},u}$ is calculated using the transformation in Equation (8).

We already stated that when magnetic balance is not used, the basis set is not explicitly dependent on the nuclear spin magnetic moment. The latter is the perturbation parameter defining first-order hyperfine properties. Therefore, with kinetic balance only, the basis set and the X2C transformation matrix elements are not explicitly dependent on the perturbation. If the X2C transformation in the absence of the perturbation is exact, and if the basis set is not explicitly dependent on the perturbation, then in variational calculations the Hellmann-Feynman theorem applies. For the calculations of a first-order (non-response) atomic and molecular property, it would then suffice to calculate the property as an expectation value of the transformed Hamiltonian derivative. In practice, the X2C transformation, as it is commonly used, is formally exact only for a one-electron problem. This introduces an approximation in calculations of many-electron systems. Then, the X2C transformation matrix elements appear effectively as non-variational parameters in the calculation, and their response is needed such that a first-order property corresponds exactly to a derivative of the approximate X2C energy. However, it is not always essential that this correspondence is established exactly. [For the energy gradients in geometry optimizations, for example, the correspondence would be essential.] For properties such as electric field gradients[50,86,87] and hyperfine coupling,[53,88] previous calculations have either shown explicitly, or implicitly by their excellent performance, that errors from neglecting the response of the X2C transformation are very small compared to the desired relativistic effects on said properties in heavy-element systems, and the sensitivity of these properties to other approximations in the calculations.

2.2 HFC Implementation within the SO-RASSI Framework

The methodology is based on mapping the pseudospin approach to matrix elements of the hyperfine interaction calculated ab-initio. The implementation for Kramers pair doublets and matrix elements of the nonrelativistic HFC operator was previously reported by our group in Reference 19, closely following the strategy for calculations of the electronic Zeeman coupling g-factors.[67,89–91]

The interaction of the electrons with the external magnetic field $\boldsymbol{B}$ is parameterized by the Zeeman spin Hamiltonian,

$$\tilde{H}^{\mathrm{Z}} = \boldsymbol{B} \cdot \mathbf{g} \cdot \tilde{\boldsymbol{S}} \tag{11}$$

which has the same formal structure as the hyperfine spin Hamiltonian parameterizing the magnetic interaction between the electron spins and a nuclear spin vector $\boldsymbol{I}_{\mathrm{N}}$,

$$\tilde{H}_{\mathrm{N}}^{\mathrm{HFC}} = \boldsymbol{I}_{\mathrm{N}} \cdot \mathbf{a}_{\mathrm{N}} \cdot \tilde{\boldsymbol{S}} \tag{12}$$

Here, $\mathbf{g}$ and $\mathbf{a}_{\mathrm{N}}$ are the g-matrix and the hyperfine coupling matrix, respectively, and $\tilde{\boldsymbol{S}}$ is the pseudospin operator. A rank-2 tensor $\mathbf{G}$ for the Zeeman interaction in terms of quantum mechanical Kramers doublet components $|i\rangle$ and $|j\rangle$ has the elements[90,92]

$$G_{uv} = (\mathbf{g}\mathbf{g}^T)_{uv} = 2 \sum_{i,j} \langle i|h_{\mathrm{N}}^{\mathrm{Z},u}|j\rangle\langle j|h_{\mathrm{N}}^{\mathrm{Z},v}|i\rangle \tag{13}$$

with $u, v, \in \{x, y, z\}$, and superscript T indicating a matrix transpose. The operator $h_{\mathrm{N}}^{\mathrm{Z},u}$ is the quantum mechanical perturbation operator for the (Zeeman) interaction with the external field, given by the derivative of the many-electron Hamiltonian with respect to B_u taken at zero field strength. The principal magnetic axes of a system, and the absolute values of the principal g-factors, are then obtained from the eigenvectors and the square roots of the eigenvalues, respectively, of $\mathbf{G}$. Based on the analogy of Equations (11) and (12), the HFC for a Kramers doublet is obtained from a matrix $\mathbf{A}$ with elements

$$A_{\mathrm{N},uv} = (\mathbf{a}_{\mathrm{N}}\mathbf{a}_{\mathrm{N}}^T)_{uv} = 2 \sum_{i,j} \langle i|h_{\mathrm{N}}^{\mathrm{HFC},u}|j\rangle\langle j|h_{\mathrm{N}}^{\mathrm{HFC},v}|i\rangle \tag{14}$$

Up to a conversion factor from nuclear spin to nuclear magnetic moment, which is taken care of in a post-processing step, the operator $h_{\mathrm{N}}^{\mathrm{HFC},u}$ is the HFC operator $\mathbf{h}_{\mathrm{X2C}}^{\mathrm{mag},u}$ from Equation (8). The electronic states in the equation are SO-RASSI wavefunctions.

Equations (8) and Equation (10) are used for calculating the X2C transformed magnetic perturbation operator matrix elements. The matrix elements of the 4-component operators $\mathbf{h}^{\mathrm{UL},u}\,\mathbf{h}^{\mathrm{LU},u}$ in Equation (10), are calculated using AO integrals which F_u is combined with ∂_v acting on the bra or ket. Due to the *a posteriori* treatment of the SO interaction in the RASSI code, the transformation matrices $\mathbf{U}^{\mathrm{UU}}$ and $\mathbf{U}^{\mathrm{UL}}$ in Equation (8) are those corresponding to a scalar relativistic X2C transformation, and the action of the Pauli spin matrices in Equations (10a),(10b) is deferred until the SO-RASSI step. That is, the matrix elements of the spin-free components of these operators between scalar relativistic spin-free RASSCF states are calculated first. The presence of a Pauli

spin matrix is taken care of during the transformation to the SO-RASSI states, in the same way that the code takes care of the Pauli spin matrices appearing in the SO coupling operator itself. In the non-relativistic limit, the transformation matrices $\mathbf{U}^{\mathrm{UU}}$ and $\mathbf{U}^{\mathrm{UL}}$ become unit matrices[93] and the SO interaction vanishes.

In Reference 94, Chibotaru and Ungur derived an extension of Equation (13) to treat states with a pseudospin $\tilde{S} > 1/2$. We therefore took the opportunity to generalize the HFC implementation to cases with $\tilde{S} > 1/2$ as well. In analogy to the **G**-tensor expression from Reference 94, the HFC and its principal axis system are calculated from the eigenvectors and the square roots of the eigenvalues of a matrix with elements

$$A^{\tilde{S}}_{\mathrm{N},uv} = \frac{6}{\tilde{S}(\tilde{S}+1)(2\tilde{S}+1)} \frac{A_{\mathrm{N},uv}}{4} \tag{15}$$

Here, $A_{\mathrm{N},uv}$ is defined formally the same as in Equation (14), but the summations now go over all components of a state with pseudospin $\tilde{S} > 1/2$. For $\tilde{S} = 1/2$, Equation (15) reverts to (14).

2.3 Calculations of the HFC contributions from different mechanism

Based on the non-relativistic theory, the magnetic dipole-dipole hyperfine structure has traditionally been interpreted to arise from three physical mechanisms, namely the Fermi-contact (FC), spin-dipole (SD) and paramagnetic spin-orbital (PSO) contribution. The latter is sometimes also labeled OP for 'orbital paramagnetic'. FC and SD arise from the magnetic interaction between the nuclear spin and the electron spin. PSO describes the magnetic interaction of the nuclear spin with the electron orbital angular momentum. Although the electron spin and orbital angular momentum couple in the relativistic theory, the structure of the operator matrices in Equations (10a),(10b) still allows to identify the PSO vs. FC+SD contributions via the spin-independent and spin-dependent terms, and FC in particular by the spin-dependent contributions with $u = v$.

Equation (8) shows that in the non-relativistic limit, when the transformation matrices become unit matrices, the HFC operator matrix is given simply by the addition of the matrix elements in Equations (10a) and (10b). The spin-independent part then reverts to the non-relativistic PSO operator matrix, with the operator being $\mu_0 e/(4\pi m) r_K^{-3} \boldsymbol{r}_K \times \boldsymbol{p}$. The addition of the spin-dependent matrix elements from Equations (10a) and (10b) gives

$$\frac{\mu_0}{4\pi}\frac{e\hbar}{2m}\sigma_u \left[(-1) \int \frac{\boldsymbol{r}_K}{r_K^3} \cdot \boldsymbol{\nabla}(\chi_\mu \chi_\nu)\, dV + \sum_v \sigma_v \int \frac{r_{K,v}}{r_K^3} \partial_u (\chi_\mu \chi_\nu)\, dV \right]$$

By using integration by parts,[95] the derivatives can be shifted from the basis function products to

the operators. The first integral in the previous equation then gives

$$\frac{\mu_0}{4\pi}\frac{e\hbar}{2m}\sigma_u \int \boldsymbol{\nabla}\cdot\frac{\boldsymbol{r}_K}{r_K^3}\,(\chi_\mu\chi_\nu)\,dV = \frac{\mu_0}{4\pi}\frac{e\hbar}{2m}4\pi\sigma_u \int \delta(\boldsymbol{r}-\boldsymbol{r}_K)(\chi_\mu\chi_\nu)\,dV$$

The $v = u$ term in the sum over v gives $-1/3$ times the same result with the Dirac delta just derived. In combination, we have a matrix element with the operator

$$\frac{\mu_0}{4\pi}\frac{e\hbar}{2m}\frac{8\pi}{3}\sigma_u\delta(\boldsymbol{r}-\boldsymbol{r}_K)$$

which is indeed the derivative of the non-relativistic FC operator with respect to the u component of the nuclear spin magnetic moment vector. The remaining part of the sum over v then gives the SD contribution to the HFC. For convenience, we opted to partition the results from the X2C calculations in the same way into PSO, FC, and SD contributions.

With different combinations of the u, v indices entering Equation (10), all three contributions can be calculated accordingly. The electron spin-independent PSO contribution appears in HFC in one of three ways: either, SOC mixes an orbitally degenerate spin state into a pure spin ground state, or the ground state is orbitally degenerate with non-zero orbital angular momentum, or there are low-energy orbitally degenerate states that are thermally populated. We do not consider the latter case further. We note in passing that the PSO contribution can also be estimated by treating the SO operator by linear response, on top of a calculation with a pure spin state.[19] However, this approach is usually limited to situations where the PSO contribution is minor.

A relativistic calculation of HFC with the non-relativistic operators introduces a picture-change error. This error is particularly large for the FC contribution. This is because of the Dirac delta, which samples the spin density directly at the nucleus. If the nuclei are treated as point nuclei, with an adequate basis set, the spin density from s (and $p_{1/2}$) orbitals centered at the nucleus have a weak singularity, leading to catastrophic failure in conjunction with an operator containing a Dirac delta singularity. In calculations with finite basis sets and finite nuclei, the use of a 'contact' operator leads to unphysically amplified FC contributions, which was noted already in our previous publication reporting the SO-RASSI implementation with non-relativistic operators.[19] The tests were therefore restricted to situations where unphysical FC contributions were likely kept under control, as already mentioned in the introduction. The X2C implementation reported herein does away with these restrictions.

3 Computational Details

Calculations were performed with a locally modified version of the open source OpenMolcas program package[73,96] interfaced with a locally modified version of the integral-derivative library GEN1INT of Gao et al.[97] The modifications were made to have the integral module of Molcas generates magnetic integrals $\langle \mu | F_u | \partial_v \nu \rangle$ for all combinations $u, v \in \{x, y, z\}$ over the primitive Gaussian-type orbital (GTO) basis functions. The integrals were then subjected to the X2C transformation as described in Section 2.1, using the transformation matrices produced by the scalar X2C module available in Molcas.[98] Subsequent contraction produced the hyperfine integrals used in the calculations. The integrals were checked against those generated by the Rys quadrature code[53,99] in NWChem.[100] In the present work, we use the nuclear potential in the X2C transformation, in conjunction with the spherical Gaussian nucleus model available in Molcas to treat finite nuclear volume effects. If desired, two-electron contributions can be added in the X2C transformation, for instance, with mean-field or model potentials in the transformation, to approximate the effects of the electron repulsion on the X2C transformation.[101–103]

As mentioned already, the SO coupling was treated via state interaction.[58,62,63] The atomic mean-field integral (AMFI) approximation was used used for the SO Hamiltonian.[64–66] It is worth mentioning that the AMFI integrals are based on a low-order Douglas-Kroll-Hess (DKH) Hamiltonian with Breit-Pauli two-electron contributions, not X2C. This treatment may be improved using more recent SO X2C mean-field approaches of Cheng and coworkers.[104,105] However, the main focus herein is avoiding the breakdown of the nonrelativistic approximation of the hyperfine operator in relativistic calculations, and the X2C-transformed magnetic integrals are fully consistent with the scalar X2C Hamiltonian used to calculate the spin-free wavefunctions prior to RASSI. We plan to introduce an X2C-based AMFI module in Molcas as part of future studies.

Optimized structures for CH_3, HSiS, SiSH, TiF_3, HgH, and HgF were taken from Reference 106 (see also Refs. 107 and 38 for DFT benchmarks using some of the same systems). The $CeCl_6$ structure was taken from Reference 108, and the NpF_6 structure is from Reference 109 and was optimized with CASPT2. All-electron correlation consistent polarized valence triple-ζ (cc-pVTZ-DK for the lighter elements and cc-pVTZ-X2C for Ce, Er and Np) basis sets were used throughout, except for the $TbPc_2$ systems (Pc = phthalocyanine dianion), for which the corresponding double-ζ basis sets were used.[110–116] The basis sets are contracted with respect to second order DKH and X2C Hamiltonian calculations, as indicated by postfixes 'DK' and 'X2C', respectively. For first and second row light elements, using the second order DKH sets introduces negligible differences compared to X2C for the purpose of this study. The truncated $TbPc_2$ structures (see below) were optimized using Kohn-Sham (KS) density functional theory (DFT) calculations with the scalar all-electron zeroth-order regular approximation (ZORA) relativistic Hamiltonian[33,117,118] provided

by Amsterdam Density Functional (ADF) program package.[119] The functional used were the 'pure' (non-hybrid) functional PBE,[120] the basis sets used were the Slater-type TZP basis sets for all elements.,[121] and the grid used for numerical integration corresponded to the 'very good'[122] setting.

The value $c = 137.036$ for the speed of light in atomic units has been utilized throughout. For calculated hyperfine coupling constants, the unit conversion from atomic units to MHz utilized the following nuclear g-factors:[123–125] $g(^{1}\mathrm{H}) = 5.5857$, $g(^{13}\mathrm{C}) = 1.4048$, $g(^{19}\mathrm{F}) = 5.2577$, $g(^{29}\mathrm{Si})$ = -1.1106, $g(^{33}\mathrm{S}) = 0.4292$, $g(^{35}\mathrm{Cl}) = 0.5479$, $g(^{47}\mathrm{Ti})$ = -0.3143, $g(^{199}\mathrm{Hg}) = 1.0118$, $g(^{141}\mathrm{Ce}) =$ 0.3143, $g(^{167}\mathrm{Er})$ = -0.1618, $g(^{159}\mathrm{Tb}) = 1.343$ and $g(^{237}\mathrm{Np}) = 1.2560$. [Note that in Reference 53, $g(^{1}\mathrm{H})$ was mis-typed with a leading 0 instead of 5.]

Spin polarization in the calculated wavefunctions was obtained in spin-unrestricted Hartree-Fock (UHF) calculations with 10^{-9} and 10^{-4} atomic units for energy and density thresholds respectively, where feasible, and by RASSCF calculations as already mentioned in the introduction. The procedure has been detailed in Refs. 19, 69, 70, and therefore only a synopsis is given here. First, a RASSCF calculation with only the unpaired electrons and orbitals in the RAS2 space were carried out. For $CeCl_6$ and Er, the 6s orbital was included in RAS2 in addition to the 4f shell, because of their closely spaced orbital energies. Inner shell spin polarization was then introduced via RAS-CI, denoted as RAS[X/Y], where X and Y are numbers of orbitals in the RAS1 and RAS3 spaces, respectively. Only single excitations were allowed among RAS1 and RAS3, to keep the calculations tractable, which means the resulting calculated state energies are not improved, and the extent of the spin polarization is likely under-estimated. Two holes / two electrons in RAS1/3 were allowed for the CH_3 radical to examine the effects of dynamic electron correlation. However, as shown in Refs. 19, 69, 70, the spin polarization introduced by the extended RAS1/3 space does resemble the spin polarization obtained in DFT calculations, for systems where a comparison can be made. It should be noted that the active spaces were selected solely based on orbital energies, i.e., there was no orbital order altering to include certain MOs preferentially. The scalar relativistic RASSCF wavefunctions thus obtained were then spin-orbit coupled via the RASSI procedure to obtain the ground state, for which the HFC was determined.

Signs of HFCCs are not usually determined in experiments. In the RASSI calculations, due to the way that the absolute values of the principal components of the HFC tensor are obtained as the square roots of the eigenvalues of the matrix in Equation (14), the sign information is lost. Individual FC, SD, and PSO sub-contributions to the HFC were determined by combining one or multiple sets of operators, FC, SD, FC+SD, and PSO. Note that because the HFC is calculated in the SO-RASSI framework via a 'square of sum' and not a 'sum of squares' fashion, the individual mechanisms do not cleanly add up to the total. However, as noted also previously,[19] cross contributions appear to be small. The signs of the FC and FC+SD contributions are then deter-

mined based on the Mulliken spin populations[126] on each nuclear site, and by comparison of the FC, SD, and FC+SD contributions with those determined straight from contracting the operator matrices with UHF spin-density matrices, which gives signed HFC contributions. The signs of PSO contributions are then given relative to FC+SD to match the total calculated HFC for cases where the sign is known, either from experiments or prior calculations, or in cases where the UHF calculations strongly indicate a negative HFC dominated by FC+SD. The HFC contributions are given with 3 to 5 significant figures to facilitate comparison. Extremely large results, obtained with the non-relativistic FC operator to emphasize the picture change effect in select cases, are given in a "$\sim 10^n$" notation.

4 Results and Discussion

The systems for testing the new X2C implementation were selected in part for continuity with our previous SO-RASSI study of HFC.[19] These molecules are the radicals CH_3, HSiS, SiSH and TiF_3, and three systems known to have particularly large relativistic effects on the HFC, namely HgH, HgF and NpF_6. This study includes three additional test systems, namely $CeCl_6^{3-}$, the Er atom, and the neutral and anionic $TbPc_2$. The ground state of Er is $^3H_6$, with a known hyperfine coupling constant, and therefore represents an interesting test for the capability to calculate the HFC for a highly degenerate state via Equation (15). $CeCl_6^{3-}$ has a simple electronic structure, and prior calculations are available for comparison. Finally, the $TbPc_2$ complex (Figure 1 shown later) and its anion were chosen because the system has attracted attention recently in the context of single-molecule magnetism,[71] and calculated HFC data were reported for the system, obtained with nonrelativistic hyperfine operators in an SO-RASSI approach that was essentially equivalent to the one of Ref. 19. Due to the large size of the ligand, truncated models for $TbPc_2$ were set up by removing peripheral atoms from the available crystal structures, and capping dangling bonds by hydrogen atoms whose positions were subsequently optimized with DFT.

Table 1 gathers the isotropic HFC constants calculated with X2C. Available experimental data are also provided in the table, or results from prior computations in case experimental data were lacking. The scalar relativistic UHF calculations did not produce the PSO contributions and should therefore be compared with the corresponding FC+SD data from the SO-RASSI calculations.

Table 1: Calculated Isotropic Hyperfine Coupling Constants (MHz) and calculated A_{zz} element for the neutral and anionic $TbPc_2$ models

		SO-RASSI					UHF	
	active space	FC	SD	FC+SD	PSO	Total	FC+SD	Lit.[a]
CH_3	$\tilde{S} = 1/2$							
C	CAS(1,8)	0.02	0.00	0.02	−0.03	−0.01	126	108[c]
C	RAS[4/60]	113	0.00	113	0.00	113		
C	RAS[4/60][b]	117	0.00	117	0.00	117		
H	CAS(1,8)	0.00	0.00	0.00	0.00	0.00	−117	−64.5[c]
H	RAS[4/60]	−58.0	0.00	−58.0	0.00	−58.0		
H	RAS[4/60][b]	−56.0	0.00	−56.0	0.00	−56.0		
HSiS	$\tilde{S} = 1/2$							
H	CAS(1,8)	190	0.00	190	0.05	190	312	335.7[d]
H	RAS[15/55]	257	0.00	257	0.08	257		
Si	CAS(1,8)	−461	0.00	−461	−0.83	−462	−528	
Si	RAS[15/55]	−468	0.00	−468	−1.13	−469		
S	CAS(1,8)	2.78	0.00	2.78	0.30	3.08	13.4	
S	RAS[15/55]	25.6	0.00	25.6	0.73	24.8		
SiSH	$\tilde{S} = 1/2$							
Si	CAS(1,8)	0.25	0.01	0.26	−3.62	−3.35	−80.5	
Si	RAS[15/55]	−60.4	0.01	−60.4	−3.86	−64.3		
S	CAS(1,8)	16.1	0.00	16.1	0.16	16.3	10.4	
S	RAS[15/55]	6.84	0.00	6.84	0.17	6.98		
H	CAS(1,8)	59.9	0.00	59.9	0.05	59.9	102	
H	RAS[15/55]	92.1	0.00	92.1	0.05	92.1		
TiF_3	$\tilde{S} = 1/2$							
Ti	CAS(1,5)	−199	0.02	−199	−3.61	−203	−160	−185[e]
Ti	CAS(3,7)	−189	0.08	−189	−8.52	−197		
Ti	RAS[14/55]	−207	0.06	−207	−7.36	−215		
F	CAS(1,5)	4.24	0.00	4.23	1.66	3.73	−42.1	−24[e]
F	CAS(3,7)	4.93	−0.01	4.92	−1.04	3.87		
F	RAS[14/55]	−23.9	−0.03	−24.0	−1.83	−25.7		
HgH	$\tilde{S} = 1/2$							
Hg	CAS(3,6)	7882	−1.79	7879	70.9	7951	8393	7002[f]
Hg	RAS[8/55]	6947	−1.49	6946	64.5	7010		*7067*[n]
H	CAS(3,6)	524	−0.02	524	0.74	525	608	710[f]
H	RAS[8/55]	628	−0.02	628	0.70	628		

HgF	$\tilde{S} = 1/2$							
Hg	CAS(3,6)	16703	−0.39	16703	22.7	16726	25210	22127[g]
Hg	RAS[8/60]	20005	−0.31	20004	20.2	20024		*18982*[o]
F	CAS(3,6)	−33.2	0.12	−33.1	−8.27	−41.4	463	578[g]
F	RAS[8/60]	413	−0.16	413	42.2	455		
Er	$\tilde{S} = 6$							
Er	CAS(14,8)	−0.07	−9.15	−9.22	−137	−146	−219	−120[h]
Er	RAS[12/40]	8.28	−9.50	−1.22	−138	−139		
Er	RAS[18/65]	20.2	−9.88	10.4	−137	−126		
$CeCl_6^{3-}$	$\tilde{S} = 1/2$							
Ce	CAS(1,8)	0.06	44.8	44.9	−254	−209	86.9	*-280*[i]
Ce	RAS[4/20]	0.06	44.9	44.9	−254	−209		*-192*[j]
Ce	RAS[12/40]	0.07	45.6	45.7	−253	−208		
Ce	RAS[18/60]	−1.66	45.4	43.7	−254	−210		
NpF_6	$\tilde{S} = 1/2$							
Np	CAS(1,7)	3.33	151	155	−1600	−1446	1888	−1995[k]
Np	RAS[12/40]	−149	161	11.8	−1691	−1679		
Np	RAS[12/65]	−283	167	−115	−1696	−1812		
Np	RAS[16/65]	−312	168	−144	−1713	−1857		
$TbPc_2^l$	$\tilde{S} = 1/2$							
Tb neutral	CAS(9,8)	14.3	770	756	6897	6141		*6146*[m]
	$\tilde{S} = 1/2$							
Tb anion	CAS(8,7)	4.68	770	774	6891	6117		*5992*[m]

[a] Literature data. In case of calculations, the corresponding values are italic. [b]Single and double excitations RAS1/3 based on the same active space definitions, see Section 3. [c]Reference 129. [d]Reference130 [e]Reference 131. [f]Reference 132. [g]1/3 of sum of $a_{\parallel}$ and $2a_{\perp}$ in Reference 133. [h]Reference 134. [i]Four-component SCF Dirac scattered wave calculation from Reference 108. [j]Two-component ZORA DFT/PBE-GGA calculation from Reference 108. [k]Reference 124 [l]Truncated $TbPc_2$ models shown in Figure 1. [m] SO-RASSI calculations using non-relativistic hyperfine integrals, Reference 72. [n] Finite nucleus scalar X2C DFT/PBE0 calculation from Reference 53. [o] Finite nucleus scalar quasi-relativistic (zeroth-order regular approximation) DFT/PBE0 calculation from Reference 107.

Table 2 further facilitates a comparison between values calculated with the aforementioned magnetic integrals and values calculated with the transformation-deactivated (picture-change uncorrected) integrals.

Table 2: Hyperfine coupling constants (MHz) calculated from X2C wavefunctions with matching transformed hyperfine integrals versus nonrelativistic hyperfine operators[a] [b]

		SO-RASSI					UHF	
	active space	FC	SD	FC+SD	PSO	Total	FC+SD	Lit.
HgH								
nonrel.								
Hg	CAS(3,6)	$\sim 10^6$	−1.79	$\sim 10^6$	104	$\sim 10^6$	$\sim 10^6$	7002
H	CAS(3,6)	524	−0.02	524	0.78	525	608	710
X2C								
Hg	CAS(3,6)	7882	−1.79	7879	70.9	7951	8393	
H	CAS(3,6)	524	−0.02	524	0.74	525	608	
HgF								
nonrel.								
Hg	CAS(3,6)	$\sim 10^6$	−0.39	$\sim 10^6$	25.3	$\sim 10^6$	$\sim 10^6$	22127
F	CAS(3,6)	−37.7	0.12	−37.6	−8.34	−45.9	485	578
X2C								
Hg	CAS(3,6)	16703	−0.39	16703	22.7	16726	25210	
F	CAS(3,6)	−33.2	0.12	−33.1	−8.27	−41.4	463	
NpF_6								
nonrel.								
Np	CAS(1,7)	0.00	154	154	−1627	−1473	$\sim 10^5$	−1995
Np	RAS[12/40]	−3602	168	−3438	−1717	−5150		
X2C								
Np	CAS(1,7)	3.33	151	155	−1600	−1446	1888	
Np	RAS[12/40]	−149	161	11.8	−1691	−1679		

[a] 'nonrel.' indicates nonrelativistic magnetic integrals used in conjunction with X2C wavefunctions. [b]The references for the experimental values are the same as those in Table 1

4.1 CH_3, HSiS, SiSH and TiF_3

For these systems in their spin-doublet ground states, the HFC is dominated by the FC mechanism. The SD contribution to the isotropic HFC is zero for a pure spin state, but it influences the tensor components. When the atoms become heavier, and SO coupling starts to play a role in the HFC, PSO contributions start to appear in the HFC, and the SD contribution to the isotropic coupling is no longer zero. These trends is clearly visible in this subset of molecules.

For CH_3, a minimal active space calculation not including the spin-polarization gives neg-

ligible HFCCs. The unpaired electron is associated with the carbon 2p orbital perpendicular to the molecular plane, and therefore does not create any spin density at the nuclei. A considerable amount of spin-polarization can be recovered with the RAS[4/60] setup, which promotes single electron excitations from the inner carbon 1s and three C-H bonding MOs. This effectively creates an excess of α-spin density at the carbon nucleus. The McConnell spin polarization mechanism[135] then leads to excess β-spin density at the protons, giving positive and negative signs for the FC contributions for the C and H respectively. The agreement of the calculated HFC constants with experimental data is good. A closer look at the composition of the RAS[4/60] ground state wavefunction indicated that the dominant determinant responsible for the spin polarization, with about 4% weight, corresponds to a β-spin hole in an orbital that is primarily carbon 1s and a β-spin electron in an orbital that has large coefficients of hydrogen 1s basis functions. The UHF calculation produces the correct sign pattern in the spin-polarization, but severely overestimates the magnitude at the protons.

Similar trends are present for several of the other HFC constants in this set of molecules: The minimal active space generates a much too small FC contribution, and the increasing RAS spaces facilitate the generation of the desired spin polarization. For an evaluation of the dynamic electron correlation effects on the HFC, calculations were also performed with two electrons / two particles in RAS1/3, using the RAS[4/60] active space for CH_3. The results are within 2 MHz of the simpler 'singles' approach, showing that—at least for this system—the chosen route for HFC calculations is able to give reasonable results at relatively low computational cost. In the CI route, a more balanced spin polarization is created by including higher substituted determinants in the wavefunction, which drives down the energy and changes the weights of the singles and other configurations.

The calculated electronic structures of the HSiS and SiSH radicals agree well with previous work.[136] The calculated HFC constants are mostly in good agreement with the previous SO-RASSI calculations[19] as far as the trends with increasing RAS space and the results with the smallest and largest active spaces are concerned. An exception is Si in HSiS for which the unsigned isotropic HFC in Ref. 19 is 611 MHz, whereas our present value is -469 MHz and closer to the hybrid DFT result (-508) given in the cited reference. The discrepancies are due to using X2C transformed HFC integrals. Table S11 shows the results for HSiS and SiSH obtained with the picture-change uncorrected hyperfine integrals. The FC contribution for Si and S atoms is exaggerated by 10 to 20%, while the SD and PSO contributions remain mostly the same and the proton HFCCs are not affected. The underestimation of the proton HFCC for HSiS compared to the experimental value is possibly due to experimental conditions that were not modeled. However, proton HFCCs were also underestimated for HXY type of molecules in the previous RASSI study,[19] compared to experiments or DFT results, which indicates insufficient spin po-

larization in the calculation. Attempts to resolve the discrepancy by an extension of RAS1/3 to two holes/electrons, further expansion of the RAS space, or by using experimentally determined structure parameters were unsuccessful, yielding results within 3 MHz of the value reported in Table 1. We tentatively attribute the discrepancy to basis set incompleteness and dynamic electron correlation effects beyond those that we attempted to model.

The present results for TiF_3 agree well with those reported in Ref. 19, which shows that the use of non-relativistic hyperfine operators did not artificially inflate the important FC contributions. The agreement with the experimental coupling constants for Ti and F is satisfactory. As for the F ligand, the CAS(1,5) and CAS(3,7) active spaces both predict α-spin population on F in all of the valence bonding orbitals, giving the opposite sign for the HFC coupling as the experiment. The RAS[14/55] active space includes the Ti-F bonding orbitals with large F 2s character. As a result, the Mulliken spin population from the fluorine s-type orbitals changes from 0.0003 to -0.0011. The excess of β-spin density associated with fluorine s orbitals then leads to good agreement with the experimental coupling constant.

4.2 Heavy element systems: HgH, HgF, Er, $CeCl_6^{3-}$ and NpF_6

Due to the utterly severe picture-change errors for HFC constants of mercury, no such results were reported in the previous SO-RASSI study.[19] In these cases, the spin density of Hg is directly associated with an unpaired orbital with large Hg 6s character, and a sampling of the relativistic spin density by a Dirac delta produces un-physical results that vary over a wide range depending on the flexibility of the basis set near the Hg nucleus. In the previous study, the reported Np hyperfine coupling was in excellent agreement with the experiment. The coupling is dominated by the PSO contribution. It was noted that the active space at the metal had to be chosen carefully such as to avoid spin polarization of s orbitals, which would have caused large picture-change errors. We take the opportunity to re-examine these cases here, along with additional heavy-element coupling constants.

The results in Table 1 for HgH and HgF clearly demonstrate that the X2C SO-RASSI results are reliable. With the RAS1/3 'singles' approach the calculated coupling constants improve nicely toward the available experimental data. The effect is rather dramatic for F in HgF. It appears that the RAS space used in Ref. 19 was still too small. It was further noted in the previous study that (i) in DFT calculations the fluorine coupling constant in HgF is very sensitive to the functional approximations, and (ii) the experimental isotropic coupling for HgF may be 578 or 318 MHz, depending on whether the reported tensor components are assumed to have the same or opposite sign. Our present best SO-RASSI coupling for F in HgF is between those two limits, but closer to 578.

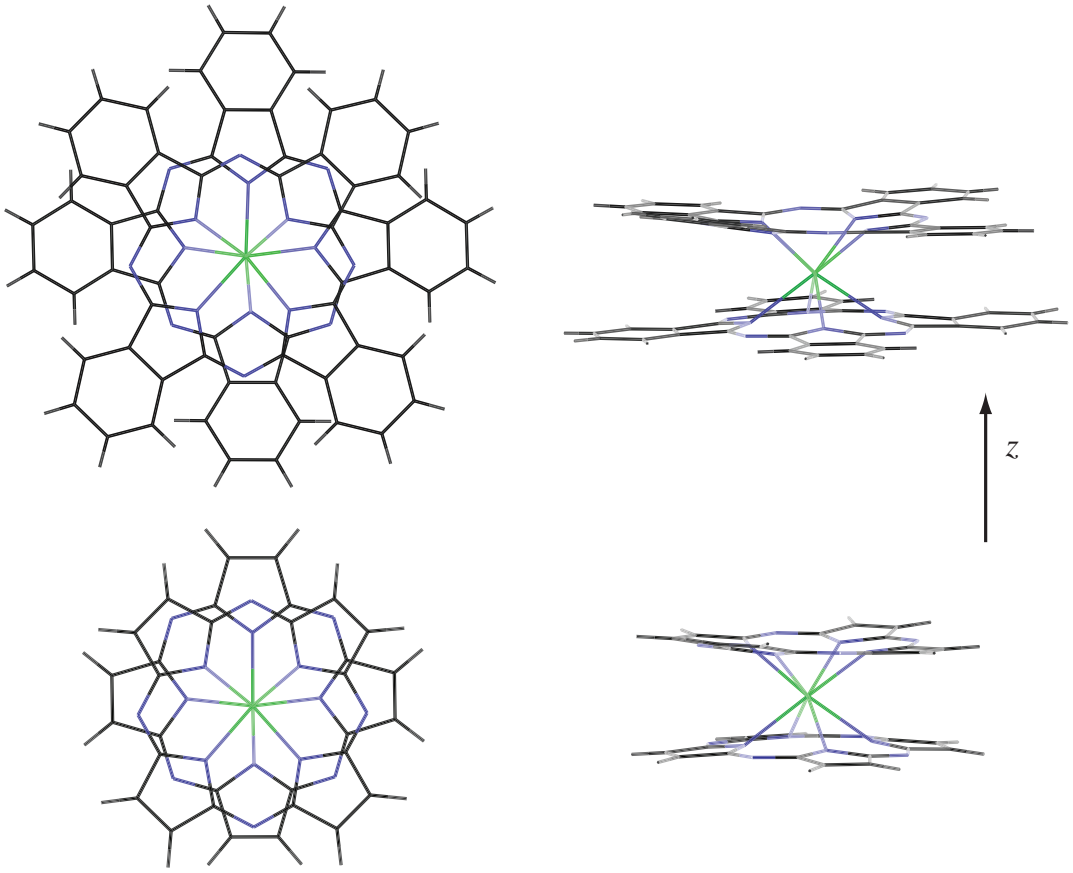

Figure 1: Side and top views of the neutral $TbPc_2$ molecules before (top) and after the truncation (bottom). The structure of the anionic system is similar and not shown. Structures were taken from Reference 127 and 128 for anionic and neutral $TbPc_2$, respectively. The center atom in green is Tb. Colors of green, black, and gray represent N, C, and H, respectively. The z direction connects the metal and the ligand centroids.

Table 2 provides data highlighting the breakdown of relativistic wavefunction calculations in conjunction with non-relativistic HFC operators for heavy-atom HFC constants. Since the comparison is for illustrative purposes only, the results for HgH and HgF are based on the small active spaces. Clearly, the Hg coupling constants with the non-relativistic operators are un-physical, whereas the proton coupling constant is not at all affected. With the chosen basis set for fluorine, the picture-change effect on its coupling constant is on the order of 10% even for this light atom.

The X2C data for the neptunium HFC in NpF_6 in Table 1 show satisfactory agreement with the experiment, with the best calculation giving a result that is a bit too low in magnitude. We decided to forego calculations of the fluorine HFC in the present study, as it turned out to be very sensitive to the chosen active space. As known from previous calculations, as already stated, the Np HFC

is strongly dominated by the PSO contribution. As a reminder, this mechanism is caused by the electron orbital angular momentum. In NpF_6, the ground state orbital angular momentum is a result of the SO coupling of the ${}^2A_{2u}$ ground spin state mainly with orbitally degenerate excited spin doublets, and as such the PSO contribution disappears without SO coupling. It was demonstrated in Ref. 19 that the presence of an isotropic SD contribution for NpF_6 is also a consequence of the SO coupling. Our present SD value, with the largest active space, is 168 MHz, in good agreement with the value of 161 reported in the previous study. PSO is -1713 MHz with X2C (present work) and -1623 reported previously. The data in Table 2 show that the differences are mainly caused by the active space selection. The picture change effect on the PSO contribution is actually rather small. Table 2 also shows that there is indeed a severe breakdown of the calculations when using non-relativistic hyperfine operators, when the active space at the metal is increased, due to an un-phsyical FC contribution. A comparison of the present X2C calculations to those reported in Ref. 19 shows that, even with the carefully chosen RAS space in the previous calculations, the results were contaminated by a too large FC contribution. Some error cancellation with a too small PSO contribution then led to near-perfect with the experiment. The present results, while slightly further from the experiment, are robust.

For atomic Er, the ground state ${}^3H_6$ state is 13-fold degenerate, which means that in Equation (15) the pseudo-spin $\tilde{S}$ is equal to 6. The CAS(14,8) active space gave the expected $6s^24f^{12}$ configuration with the α-spin population contained in the 4f orbitals. As a result, only SD and PSO terms contributed to the HFC constant, with the isotropic SD appearing because of SOC. The RAS[12/40] active space included the 4p,5s,4d, and 5p orbitals, in addition to 4f and 5s in RAS2. The RAS[18/65] active space further included the 4s3d orbitals. The increased active space leads to an improvement of the HFC constant toward the experiment, by generating a positive FC contribution via spin polarization of the atomic outer core shells that cancels part of the dominant PSO contribution. Since the scalar relativistic ground state, ${}^3H$, does have a large orbital angular momentum, PSO is not primarily due to SO coupling. Quenching the AMFI spin-orbit integrals for Er produces a 33-fold degenerate ground state corresponding to the 11 times 3-fold orbital and spin degeneracy of the ${}^3H$ term. The HFC calculation accordingly produces a sizable PSO contribution, close to the total calculated HFC (54 MHz magnitude). The latter is smaller than that calculated for the SO ${}^3H_6$ level, mainly because of the large degeneracy of the term. We note in passing that the report of the measured HFC constant[134] cited in Table 1 was accompanied by theoretical results from a multi-configuration Dirac-Fock electronic structure method, which also produced close agreement with the experiment upon introducing a RAS partitioning not unlike ours to generate spin polarization.

The ground state of the $CeCl_6^{3-}$ complex is conceptually similar to that of NpF_6, in that a single un-paired electron is associated mainly with a non-bonding a_{2u} valence f orbital. Therefore,

similar to NpF_6, the SO coupling then creates a dominant PSO contribution to the HFC constant, along with a secondary SD contribution. As seen in Table 1, the absolute values of the coupling contributions are smaller for $CeCl_6^{3-}$ than for NpF_6. This is in part simply because the nuclear g factor for ^{237}Np is about four times that of ^{141}Ce. This difference accounts essentially for the different values of the SD contribution in the two molecules. However, as seen in the nearly seven times different PSO contributions, the different results for the two complexes are not only attributable to the ratio of the nuclear g factors. The stronger SO coupling in the Np 5f shell surely plays an important role as well, and so do the somewhat different ligand fields.

4.3 Neutral and anionic $TbPc_2$

Our calculations for the $TbPc_2$ systems were conducted to confirm that previously reported SO-RASSI calculations[72] with non-relativistic hyperfine operators did not suffer from large picture-change errors, and to show the applicability of the X2C implementation to systems of interest in the molecular magnetism and quantum information science fields—albeit with truncated models of the ligands. Only the component of the hyperfine coupling tensor along the rotational axis of the complex, denoted z in Figure 1, is of interest. The perpendicular tensor components are negligible. The X2C results are close to those reported in Reference 72 for the following reason: The small active spaces do not allow for significant spin polarization to be generated in the metal's valence and outer core s orbitals. Significant spin polarization, however, would likely lead to a breakdown of the HFC tensor, when non-relativistic hyperfine operators are used, similar to that seen for NpF_6 in Table 2.

5 Conclusion

The purpose of the present study was two-fold. First, we showed the general applicability of RASSCF and SO-RASSI calculations for the purpose of determining electron-nucleus hyperfine coupling constants. The approach works reasonably well across the set of systems used for testing. Nonetheless, for simple radicals, density functional and coupled-cluster theory are likely to remain the methods of choice, because they treat the spin polarization in a 'black box' fashion along with the dynamic correlation. Caveats remain with those methods, too, such as spin contamination in DFT. The SO-RASSI approach becomes an attractive—or preferred—alternative in more difficult cases with spatial degeneracies or SO coupling, i.e. when the wavefunctions acquire pronounced multi-reference character.

Second, we showed that the relativistic X2C framework used for the present study offers a straightforward and simple solution to the problems that plagued a previous SO-RASSI imple-

mentation with nonrelativistic hyperfine operators. Somewhat unexpectedly, the X2C results for NpF_6 show that even with the carefully limited active space used in the previous study to determine the metal HFC constant, it appears that the previous results were contaminated by picture-change errors from the FC contribution.

The HFC operator matrix was obtained with the X2C transformation used for the one-electron Hamiltonian in the absence of magnetic fields. For many-electron systems, this is an approximation. However, the present results, as well as those from a previous DFT study based on the same approach, indicate that the approximation is not severe, especially when compared to other factors to which hyperfine coupling is sensitive, such as the dynamic electron correlation. Note, that the X2C transformed HFC operator matrices can also be used straightforwardly for calculating important contributions to the NMR chemical shift that arise in paramagnetic molecules,[68] in a module that our group developed previously in Molcas / OpenMolcas using the non-relativistic operators.[69,70] Eventually, we plan to release the code underlying the present calculations in open-source form as part of OpenMolcas.

Conflicts of interest

There are no conflicts to declare.

Acknowledgements

The authors acknowledge financial support from the U.S. Department of Energy, Office of Basic Energy Sciences, Materials and Chemical Sciences Research for Quantum Information Science, grant no. DE-SC0020169. The authors declare no competing financial interest.

Supporting Information

Supporting Information (SI) available: XYZ coordinates for all molecules. Additional calculated data for HSiS and SiSH.

Table of Contents Graphics

spin density

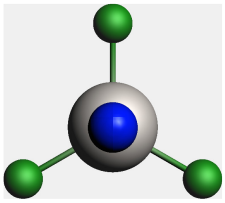

CAS(1,7)-SR

TiF_3 $\longrightarrow$

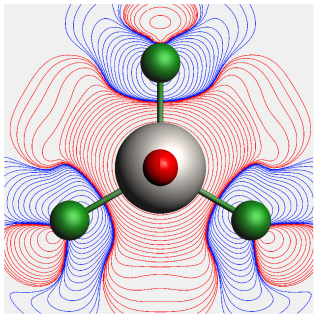

RAS[14/55]-SO

References

[1] Atherton, N. M. *Principles of Electron Spin Resonance;* Ellis Horwood series in physical chemistry Prentice Hall: New York, 1993.

[2] Eriksson, L. A. ESR Hyperfine Calculations. In *Encyclopedia of Computational Chemistry*; von Ragué Schleyer, P., Ed.; Wiley: Chichester, UK, 1998 952–958.

[3] Rieger, P. H. *Electron spin resonance. Analysis and interpretation;* The Royal Society of Chemistry: Cambridge, UK, 2007.

[4] Harriman, J. E. *Theoretical foundations of electron spin resonance;* Academic Press: New York, 1978.

[5] Kaupp, M.; Bühl, M.; Malkin, V. G., Eds.; *Calculation of NMR and EPR Parameters. Theory and Applications;* Wiley-VCH: Weinheim, 2004.

[6] Bagus, P. S.; Liu, B.; Schaefer, H. F. Study of the Contact-Term Contribution to the Hyperfine Structure Obtained from Spin-Unrestricted Hartree-Fock Wave Functions. *Phys. Rev. A* **1970**, *2*, 555–560.

[7] Munzarová, M.; Kaupp, M. A critical validation of density functional and coupled cluster approaches for the calculation of EPR hyperfine coupling constants in transition metal complexes. *J. Phys. Chem. A* **1999**, *103*, 9966–9983.

[8] Schattenberg, C. J.; Maier, T. M.; Kaupp, M. Lessons from the Spin-Polarization/Spin-Contamination Dilemma of Transition-Metal Hyperfine Couplings for the Construction of Exchange-Correlation Functionals. *J. Chem. Theory Comput.* **2018**, *14*, 5653–5672.

[9] Kristiansen, P.; Veseth, L. Many-body calculations of hyperfine constants in diatomic molecules. I. The ground state of ^{16}OH. *J. Chem. Phys.* **1986**, *84*, 2711–2719.

[10] Momose, H. T.; Nakatsuji; Shida, T. Calculation of isotropic hyperfine coupling constants by the symmetry adapted cluster expansion configuration interaction theory. *J. Chem. Phys.* **1988**, *89*, 4185–4192.

[11] Carmichael, I. Ab initio coupled-cluster calculations of isotropic hyperfine splitting in some diatomic hydrides. *J. Phys. Chem.* **1990**, *94*, 5734–5740.

[12] Perera, S. A.; Watt, J. D.; Bartlett, R. J. A theoretical study of Hyperfine Coupling Constants. *J. Chem. Phys.* **1994**, *100*, 1425–2434.

[13] Kossmann, S.; Neese, F. Correlated ab Initio Spin Densities for Larger Molecules: Orbital-Optimized Spin-Component-Scaled MP2 Method. *J. Phys. Chem. A* **2010**, *114*, 11768–11781.

[14] Datta, D.; Gauss, J. Communication: Spin densities within a unitary group based spin-adapted open-shell coupled-cluster theory: Analytic evaluation of isotropic hyperfine-coupling constants for the combinatoric open-shell coupled-cluster scheme. *J. Chem. Phys.* **2015**, *143*, 011101.

[15] Fernandez, B.; Jørgensen, P.; Byberg, J.; Olsen, J.; Helgaker, T.; Jensen, H. J. A. Spin polarization in restricted electronic structure theory: Multiconfiguration self-consistent-field calculations of hyperfine coupling constants. *J. Chem. Phys.* **1992**, *97*, 3412–3419.

[16] Feller, D.; Davidson, E. R. A multireference CI determination of the isotropic Hyperfine Constants for first row atoms B–F. *J. Chem. Phys.* **1988**, *88*, 7580–7587.

[17] Engels, B. Estimation of the influence of the configurations neglected within truncated multireference CI wavefunctions on molecular properties. *Chem. Phys. Lett.* **1991**, *179*, 398–404.

[18] Engels, B. A detailed study of the configuration selected multireference configuration interaction method combined with perturbation theory to correct the wave function. *J. Chem. Phys.* **1994**, *100*, 1380–1386.

[19] Sharkas, K.; Pritchard, B.; Autschbach, J. Effects from spin-orbit coupling on electron-nucleus hyperfine coupling calculated at the restricted active space level for Kramers doublets. *J. Chem. Theory Comput.* **2015**, *11*, 538–549.

[20] Shiozaki, T.; Yanai, T. Hyperfine Coupling Constants from Internally Contracted Multireference Perturbation Theory. *J. Chem. Theory Comput.* **2016**, *12*, 4347–4351.

[21] Datta, D.; Gauss, J. Accurate Prediction of Hyperfine Coupling Tensors for Main Group Elements Using a Unitary Group Based Rigorously Spin-Adapted Coupled-Cluster Theory. *J. Chem. Theory Comput* **2019**, *15*, 1572–1592.

[22] Wouters, S.; van Neck, D. The density matrix renormalization group for ab initio quantum chemistry. *Eur. J. Phys. D* **2014**, *68*, 272–291.

[23] Yanai, T.; Kurashige, Y.; Mizukami, W.; Chalupský, J.; Nguyen Lan, T.; Saitow, M. Density Matrix Renormalization Group for ab initio Calculations and Associated Dynamic

Correlation Methods: A Review of Theory and Applications. *Int. J. Quantum Chem.* **2015**, *115*, 283–299.

[24] Lan, T. N.; Kurashige, Y.; Yanai, T. Toward Reliable Prediction of Hyperfine Coupling Constants Using Ab Initio Density Matrix Renormalization Group Method: Diatomic $^2\Sigma$ and Vinyl Radicals as Test Cases. *J. Chem. Theory Comput.* **2014**, *10*, 1953–1967.

[25] Pyykkö, P. Relativistic Effects in Chemistry: More Common Than You Thought. *Annu. Rev. Phys. Chem.* **2012**, *63*, 45–64.

[26] Autschbach, J. Perspective: Relativistic Effects. *J. Chem. Phys.* **2012**, *136*, 150902.

[27] Visscher, L. Magnetic Balance and Explicit Diamagnetic Expressions for Nuclear Magnetic Resonance Shielding Tensors. *Adv. Quantum Chem.* **2005**, *48*, 369–381.

[28] Komorovsky, S.; Repisky, M.; Malkina, O. L.; Malkin, V. G.; Malkin, I.; Kaupp, M. Resolution of identity Dirac-Kohn-Sham method using the large component only: Calculations of g-tensor and hyperfine tensor. *J. Chem. Phys.* **2006**, *124*, 084108–8.

[29] Ilias, M.; Saue, T.; Enevoldsen, T.; Jensen, H. J. A. Gauge origin independent calculations of nuclear magnetic shieldings in relativistic four-component theory. *J. Chem. Phys.* **2009**, *131*, 124119–13.

[30] Repisky, M.; Komorovsky, S.; Malkin, E.; Malkina, O. L.; Malkin, V. G. Relativistic four-component calculations of electronic g-tensors in the matrix Dirac-Kohn-Sham framework. *Chem. Phys. Lett.* **2010**, *488*, 94–97.

[31] Komorovsky, S.; Repisky, M.; Malkina, O. L.; Malkin, V. G.; Ondik, I. M.; Kaupp, M. A fully relativistic method for calculation of nuclear magnetic shielding tensors with a restricted magnetically balanced basis in the framework of the matrix Dirac-Kohn-Sham equation. *J. Chem. Phys.* **2008**, *128*, 104101.

[32] Olejniczak, M.; Bast, R.; Saue, T.; Pecul, M. A simple scheme for magnetic balance in four-component relativistic Kohn-Sham calculations of nuclear magnetic resonance shielding constants in a Gaussian basis. *J. Chem. Phys.* **2012**, *136*, 014108–13 Erratum: J. Chem. Phys. 136, 239902 (2012).

[33] van Lenthe, E.; Baerends, E. J.; Snijders, J. G. Relativistic regular two-component Hamiltonians. *J. Chem. Phys.* **1993**, *99*, 4597–4610.

[34] Wolf, A.; Reiher, M.; Hess, B. Transgressing theory boundaries: The generalized Douglas–Kroll transformation. In *Recent Advances in Relativistic Molecular Theory*, Vol. 5; Hirao, K.; Ishikawa, Y., Eds.; World Scientific: Singapore, 2004 137–190.

[35] Reiher, M.; Wolf, A. *Relativistic quantum chemistry. The fundamental theory of molecular science;* Wiley-VCH: Weinheim, second ed.; 2015.

[36] van Lenthe, E.; van der Avoird, A.; Wormer, P. E. S. Density functional calculations of molecular hyperfine interactions in the zero order regular approximation for relativistic effects. *J. Chem. Phys.* **1998**, *108*, 4783–4796.

[37] Autschbach, J.; Patchkovskii, S.; Pritchard, B. Calculation of hyperfine tensors and paramagnetic NMR shifts using the relativistic zeroth-order regular approximation and density functional theory. *J. Chem. Theory Comput.* **2011**, *7*, 2175–2188.

[38] Verma, P.; Autschbach, J. Relativistic density functional calculations of hyperfine coupling with variational versus perturbational treatment of spin-orbit coupling. *J. Chem. Theory Comput.* **2013**, *9*, 1932–1948.

[39] Malkin, E.; Malkin, I.; Malkina, O. L.; Malkin, V. G.; Kaupp, M. Scalar relativistic calculations of hyperfine coupling tensors using the Douglas-Kroll-Hess method with a finite-size nucleus model. *Phys. Chem. Chem. Phys.* **2006**, *8*, 4079 – 4085.

[40] Luber, S.; Ondik, I. M.; Reiher, M. Electromagnetic fields in relativistic one-particle equations. *Chem. Phys.* **2009**, *356*, 205–218.

[41] Seino, J.; Hada, M. Magnetic shielding constants calculated by the infinite-order Douglas-Kroll-Hess method with electron-electron relativistic corrections. *J. Chem. Phys.* **2010**, *132*, 174105–8.

[42] Hayami, M.; Seino, J.; Nakai, H. Gauge-origin independent formalism of two-component relativistic framework based on unitary transformation in nuclear magnetic shielding constant. *J. Chem. Phys.* **2018**, *148*, 114109.

[43] Dyall, K. G. Interfacing relativistic and nonrelativistic methods. I. Normalized elimination of the small component in the modified Dirac equation. *J. Chem. Phys.* **1997**, *106*, 9618–9626.

[44] Kutzelnigg, W.; Liu, W. Quasirelativistic theory equivalent to fully relativistic theory. *J. Chem. Phys.* **2005**, *123*, 241102–4.

[45] Ilias, M.; Saue, T. An infinite-order two-component relativistic Hamiltonian by a simple one-step transformation. *J. Chem. Phys.* **2007**, *126*, 064102.

[46] Liu, W.; Peng, D. Exact two-component Hamiltonians revisited. *J. Chem. Phys.* **2009**, *131*, 031104–4.

[47] Saue, T. Relativistic Hamiltonians for Chemistry: A Primer. *ChemPhysChem* **2011**, *12*, 3077–3094.

[48] Liu, W. Essentials of relativistic quantum chemistry. *J. Chem. Phys.* **2020**, *152*, 180901.

[49] Cheng, L.; Gauss, J. Analytic second derivatives for the spin-free exact two-component theory. *J. Chem. Phys.* **2011**, *135*, 244104–8.

[50] Cheng, L.; Gauss, J. Analytic energy gradients for the spin-free exact two-component theory using an exact block diagonalization for the one-electron Dirac Hamiltonian. *J. Chem. Phys.* **2011**, *135*, 084114–7.

[51] Xiao, Y.; Liu, W.; Autschbach, J. Relativistic theories of NMR shielding. In *Handbook of Relativistic Quantum Chemistry*; Liu, W., Ed.; Springer: Berlin, 2017 657–692.

[52] Sun, Q.; Xiao, Y.; Liu, W. Exact two-component relativistic theory for NMR parameters: General formulation and pilot application. *J. Chem. Phys.* **2012**, *137*, 174105–20.

[53] Autschbach, J. Relativistic effects on electron-nucleus hyperfine coupling studied with an 'exact 2-component' (X2C) method. *J. Chem. Theory Comput.* **2017**, *13*, 710–718.

[54] Cheng, L.; Gauss, J.; Stanton, J. F. Treatment of scalar-relativistic effects on nuclear magnetic shieldings using a spin-free exact-two-component approach. *J. Chem. Phys.* **2013**, *139*, 054105.

[55] Yoshizawa, T.; Zou, W.; Cremer, D. Calculations of atomic magnetic nuclear shielding constants based on the two-component normalized elimination of the small component method. *J. Chem. Phys.* **2017**, *146*, 134109.

[56] Yoshizawa, T.; Hada, M. Calculations of nuclear magnetic shielding constants based on the exact two-component relativistic method. *J. Chem. Phys.* **2017**, *147*, 154104.

[57] Franzke, Y. J.; Weigend, F. NMR Shielding Tensors and Chemical Shifts in Scalar-Relativistic Local Exact Two-Component Theory. *J. Chem. Theory Comput.* **2019**, *15*, 1028–1043.

[58] Malmqvist, P. Å.. Calculation of transition density matrices by nonunitary orbital transformations. *Int. J. Quantum Chem.* **1986**, *30*, 479–494.

[59] Ma, D.; Li Manni, G.; Gagliardi, L. The generalized active space concept in multiconfigurational self-consistent field methods. *J. Chem. Phys.* **2011**, *135*, 044128.

[60] Roos, B. O.; Taylor, P. R.; Siegbahn, P. E. M. A Complete Active Space SCF method (CASSCF) using a density matrix formulated super-CI approach. *Chem. Phys.* **1980**, *48*, 157–173.

[61] Roos, B. O. The Complete Active Space Self-Consistent Field method and its applications in electronic structure calculations. *Adv. Chem. Phys.* **1987**, *69*, 399–445.

[62] Malmqvist, P. Å..; Roos, B. The CASSCF state interaction method. *Chem. Phys. Letters* **1989**, *155*, 189 – 194.

[63] Malmqvist, P.-A.; Roos, B. O.; Schimmelpfennig, B. The restricted active space (RAS) state interaction approach with spin-orbit coupling. *Chem. Phys. Lett.* **2002**, *357*, 230–240.

[64] Heß, B. A.; Marian, C. M.; Wahlgren, U.; Gropen, O. A mean–field spin–orbit method applicable to correlated wavefunctions. *Chem. Phys. Lett.* **1996**, *251*, 365–371.

[65] Christiansen, O.; Gauss, J.; Schimmelpfennig, B. Spin-orbit coupling constants from coupled-cluster response theory. *Phys. Chem. Chem. Phys.* **2000**, *2*, 965–971.

[66] Vahtras, O.; Engström, M.; Schimmelpfennig, B. Electronic g-tensors obtained with the mean-field spin-orbit Hamiltonian. *Chem. Phys. Lett.* **2002**, *351*, 424–430.

[67] Bolvin, H. An Alternative Approach to the g-Matrix: Theory and Applications. *ChemPhysChem* **2006**, *7*, 1575–1589.

[68] Van den Heuvel, W.; Soncini, A. NMR chemical shift as analytical derivative of the Helmholtz free energy. *J. Chem. Phys.* **2013**, *138*, 054113.

[69] Gendron, F.; Autschbach, J. Ligand NMR chemical shift calculations for paramagnetic metal complexes: $5f^1$ vs. $5f^2$ actinides. *J. Chem. Theory Comput.* **2016**, *12*, 5309–5321.

[70] Gendron, F.; Sharkas, K.; Autschbach, J. Calculating NMR Chemical Shifts for Paramagnetic Metal Complexes from First-Principles. *J. Phys. Chem. Lett.* **2015**, *6*, 2183–2188.

[71] Wysocki, A. L.; Park, K. Hyperfine and quadrupole interactions for Dy isotopes in DyPc2 molecules. *J. Condens. Matter Phys.* **2020**, *32*, 274002.

[72] Wysocki, A. L.; Park, K. Nature of Hyperfine Interactions in TbPc2 Single-Molecule Magnets: Multiconfigurational Ab Initio Study. *Inorg. Chem.* **2020**, *59*, 2771–2780.

[73] Galván, I. F.; Vacher, M.; Alavi, A.; Angeli, C.; Aquilante, F.; Autschbach, J.; Bao, J. J.; Bokarev, S. I.; Bogdanov, N. A.; Carlson, R. K. *et al.* OpenMolcas: From Source Code to Insight. *J. Chem. Theory Comput.* **2019**, *15*, 5925–5964.

[74] Dyall, K. G. An exact separation of the spin-free and spin-dependent terms in the Dirac-Coulomb-Breit Hamiltonain. *J. Chem. Phys.* **1994**, *100*, 2118–2127.

[75] Ishikawa, Y.; Binning, R. C.; Sando, K. M. Dirac–Fock discrete-basis calculations on the beryllium atom. *Chem. Phys. Lett.* **1983**, *101*, 111–114.

[76] Stanton, R. E.; Havriliak, S. Kinetic balance: A partial solution to the problem of variational safety in Dirac calculations. *J. Chem. Phys.* **1984**, *81*, 1910–1918.

[77] Sun, Q.; Liu, W.; Kutzelnigg, W. Comparison of restricted, unrestricted, inverse, and dual kinetic balances for four-component relativistic calculations. *Theor. Chem. Acc.* **2011**, *129*, 423–436.

[78] Komorovsky, S.; Repisky, M.; Malkina, O. L.; Malkin, V. G.; Malkin Ondík, I.; Kaupp, M. A fully relativistic method for calculation of nuclear magnetic shielding tensors with a restricted magnetically balanced basis in the framework of the matrix Dirac–Kohn–Sham equation. *J. Chem. Phys.* **2008**, *128*, 104101–15.

[79] Repisky, M.; Komorovsky, S.; Malkina, O. L.; Malkin, V. G. Restricted magnetically balanced basis applied for relativistic calculations of indirect nuclear spin-spin coupling tensors in the matrix Dirac–Kohn–Sham framework. *Chem. Phys.* **2009**, *356*, 236–242.

[80] Bohr, A.; Weisskopf, V. F. The influence of nuclear structure on the hyperfine structure of heavy elements. *Phys. Rev.* **1950**, *77*, 94–98.

[81] Hennum, A. C.; Klopper, W.; Helgaker, T. Direct perturbation theory of magnetic properties and relativistic corrections for the point nuclear and the Gaussian nuclear models. *J. Chem. Phys.* **2001**, *115*, 7356–7363.

[82] Autschbach, J. Magnitude of finite nucleus size effects in relativistic density functional computations of indirect NMR nuclear spin–spin coupling tensors. *ChemPhysChem* **2009**, *10*, 2274–2283.

[83] Visscher, L.; Dyall, K. G. DIRAC–FOCK ATOMIC ELECTRONIC STRUCTURE CALCULATIONS USING DIFFERENT NUCLEAR CHARGE DISTRIBUTIONS. *At. Data Nucl. Data Tables* **1997**, *67*, 207–224.

[84] Andrae, D. Finite nuclear charge density distributions in electronic structure calculations for atoms and molecules. *Phys. Rep.* **2000**, *336*, 413–527.

[85] Enevoldsen, T.; Visscher, L.; Saue, T.; Jensen, H. J. A.; Oddershede, J. Relativistic four-component calculations of indirect nuclear spin-spin couplings in MH_4 (M=C, Si, Ge, Sn, Pb) and $Pb(CH_3)H$. *J. Chem. Phys.* **2000**, *112*, 3493–3498.

[86] Mastalerz, R.; Barone, G.; Lindh, R.; Reiher, M. Analytic high-order Douglas-Kroll-Hess electric field gradients. *J. Chem. Phys.* **2007**, *127*, 074105.

[87] Autschbach, J.; Peng, D.; Reiher, M. Two-component relativistic calculations of electric-field gradients using exact decoupling methods: Spin-orbit and picture-change effects. *J. Chem. Theory Comput.* **2012**, *8*, 4239–4248.

[88] Filatov, M.; Zou, W.; Cremer, D. Analytic Calculation of Isotropic Hyperfine Structure Constants Using the Normalized Elimination of the Small Component Formalism. *J. Phys. Chem. A* **2012**, *116*, 3481–3486.

[89] Vancoillie, S.; Malmqvist, P.-A.; Pierloot, K. Calculation of EPR g tensors for transition-metal complexes based on multiconfigurational perturbation theory (CASPT2). *ChemPhysChem* **2007**, *8*, 1803.

[90] Gerloch, M.; McMeeking, R. F. Paramagnetic properties of unsymmetrical transition-metal complexes. *J. Chem. Soc., Dalton Trans.* **1975**, 2443–2451.

[91] Bolvin, H.; Autschbach, J. Relativistic methods for calculating Electron Paramagnetic Resonance (EPR) parameters. In *Handbook of Relativistic Quantum Chemistry*; Liu, W., Ed.; Springer: Berlin, 2017 725–763.

[92] Abragam, A.; Bleaney, B. *Electron paramagnetic resonance of transition ions;* Clarendon Press: Oxford, 1970.

[93] Peng, D.; Reiher, M. Local relativistic exact decoupling. *J. Chem. Phys.* **2012**, *136*, 244108–11.

[94] Chibotaru, L. F.; Ungur, L. Ab initio calculation of anisotropic magnetic properties of complexes. I. Unique definition of pseudospin Hamiltonians and their derivation. *J. Chem. Phys.* **2012**, *137*, 064112–22.

[95] Kutzelnigg, W. Origin and meaning of the Fermi contact interaction. *Theor. Chim. Acta* **1988**, *73*, 173–200.

[96] Aquilante, F.; Autschbach, J.; Baiardi, A.; Battaglia, S.; Borin, V. A.; Chibotaru, L. F.; Conti, I.; De Vico, L.; Delcey, M.; Fdez. Galván, I. *et al.* Modern quantum chemistry with [Open]Molcas. *J. Chem. Phys.* **2020**, *152*, 214117.

[97] Gao, B.; Thorvaldsen, A. J.; Ruud, K. GEN1INT: A unified procedure for the evaluation of one-electron integrals over Gaussian basis functions and their geometric derivatives. *Int. J. Quantum Chem.* **2011**, *111*, 858.

[98] Peng, D.; Reiher, M. Exact decoupling of the relativistic Fock operator. *Theor. Chem. Acc.* **2012**, *131*, 1081.

[99] Dupuis, M. New integral transforms for molecular properties and application to a massively parallel GIAO–SCF implementation. *Comp. Phys. Comm.* **2001**, *134*, 150–166.

[100] Aprà, E. *et al.* NWChem: Past, present, and future. *J. Chem. Phys.* **2020**, *152*, 184102.

[101] van Wüllen, C.; Michauk, C. Accurate and efficient treatment of two-electron contributions in quasirelativistic high-order Douglas–Kroll density-functional calculations. *J. Chem. Phys.* **2005**, *123*, 204113.

[102] Liu, W.; Kutzelnigg, W. Quasirelativistic theory. II. Theory at matrix level. *J. Chem. Phys.* **2007**, *126*, 114107.

[103] Peng, D.; Liu, W.; Xiao, Y.; Cheng, L. Making four- and two-component relativistic density functional methods fully equivalent based on the idea of "from atoms to molecule". *J. Chem. Phys.* **2007**, *127*, 104106.

[104] Liu, J.; Cheng, L. An atomic mean-field spin-orbit approach within exact two-component theory for a non-perturbative treatment of spin-orbit coupling. *J. Chem. Phys.* **2018**, *148*, 144108.

[105] Cheng, L.; Gauss, J. Perturbative treatment of spin-orbit coupling within spin-free exact two-component theory. *J. Chem. Phys.* **2014**, *141*, 164107.

[106] Aquino, F.; Govind, N.; Autschbach, J. Scalar relativistic computations of nuclear magnetic shielding and g-shifts with the zeroth-order regular approximation and range-separated hybrid density functionals. *J. Chem. Theory Comput.* **2011**, *7*, 3278–3292.

[107] Aquino, F.; Pritchard, B.; Autschbach, J. Scalar relativistic computations and localized orbital analysis of nuclear hyperfine coupling and paramagnetic NMR chemical shifts. *J. Chem. Theory Comput.* **2012**, *8*, 598–609.

[108] Ferraro, F.; Arratia-Pérez, R. Spin-orbit effects on the optical and magnetic properties of cerium (III) hexahalides. *Polyhedron* **2011**, *30*, 860–863.

[109] Notter, F.-P.; Bolvin, H. Optical and magnetic properties of the $5f^1$ AnX_6^{q-} series: A theoretical study. *J. Chem. Phys.* **2009**, *130*, 184310–11.

[110] Dunning Jr., T. H. Gaussian basis sets for use in correlated molecular calculations. I. The atoms boron through neon and hydrogen. *J. Chem. Phys.* **1989**, *90*, 1007.

[111] de Jong, W. A.; Harrison, R. J.; Dixon, D. A. Parallel Douglas–Kroll energy and gradients in NWChem: Estimating scalar relativistic effects using Douglas–Kroll contracted basis sets. *J. Chem. Phys.* **2001**, *114*, 48–53.

[112] Dunning Jr., T. H.; Peterson, K. A.; Wilson, A. K. Gaussian basis sets for use in correlated molecular calculations. X. The atoms aluminum through argon revisited. *J. Chem. Phys.* **2001**, *114*, 9244–9253.

[113] Peterson, K.; Puzzarini, C. Systematically convergent basis sets for transition metals. II. Pseudopotential-based correlation consistent basis sets for the group 11 (Cu, Ag, Au) and 12 (Zn, Cd, Hg) elements. *Theor. Chem. Acc.* **2005**, *114*, 283–296.

[114] Balabanov, N. B.; Peterson, K. A. Systematically convergent basis sets for transition metals. I. All-electron correlation consistent basis sets for the 3d elements Sc–Zn. *J. Chem. Phys.* **2005**, *123*, 64107.

[115] Lu, Q.; Peterson, K. A. Correlation consistent basis sets for lanthanides: The atoms La–Lu. *J. Chem. Phys* **2016**, *145*, 054111.

[116] Feng, R.; Peterson, K. A. Correlation consistent basis sets for actinides. II. The atoms Ac and Np–Lr. *J. Chem. Phys.* **2017**, *147*, 084108.

[117] van Lenthe, E.; Baerends, E. J.; Snijders, J. G. Relativistic total energy using regular approximations. *J. Chem. Phys.* **1994**, *101*, 9783–9792.

[118] van Lenthe, E.; Ehlers, A.; Baerends, E. J. Geometry optimizations in the zero order regular approximation for relativistic effects. *J. Chem. Phys.* **1999**, *110*, 8943–8953.

[119] Baerends, E. J.; Ziegler, T.; Atkins, A. J.; Autschbach, J.; Bashford, D.; Baseggio, O.; Bérces, A.; Bickelhaupt, F. M.; Bo, C.; Boerritger, P. M. *et al.* "ADF2017, SCM, Theoretical Chemistry, Vrije Universiteit, Amsterdam, The Netherlands, https://www.scm.com", .

[120] Perdew, J. P.; Burke, K.; Ernzerhof, M. Generalized Gradient Approximation Made Simple. *Phys. Rev. Lett.* **1996**, *77*, 3865–3868.

[121] van Lenthe, E.; Baerends, E. J. Optimized Slater–type basis sets for the elements 1 – 118. *J. Comput. Chem.* **2003**, *24*, 1142–1156.

[122] Franchini, M.; Philipsen, P. H. T.; Visscher, L. The Becke Fuzzy Cells Integration Scheme in the Amsterdam Density Functional Program Suite. *J. Comput. Chem.* **2013**, *34*, 1819–1827.

[123] Neese, F.; Solomon, E. I. Interpretation and Calculation of Spin-Hamiltonian Parameters in Transition Metal Complexes. In *Magnetism: Molecules to Materials IV*; John Wiley & Sons, Ltd: 2003; Chapter 9, 400.

[124] Butler, J. E.; Hutchison, C. A. Jr. Electron paramagnetic resonance and electron nuclear double resonance of 237-neptunium hexafluoride in uranium hexafluoride single crystals. *J. Chem. Phys.* **1981**, *74*, 3102–3119.

[125] Stone, N. "Table of Nuclear Magnetic Dipole and Electric Quadrupole Moments, International Atomic Energy Agency publication INDC(NDS)-0658", 2014.

[126] Mulliken, R. S. Electronic Population Analysis on LCAO-MO Molecular Wave Functions. I. *J. Chem. Phys.* **1955**, *23*, 1833–1840.

[127] Branzoli, F.; Carretta, P.; Filibian, M.; Zoppellaro, G.; Graf, M. J.; Galan-Mascaros, J. R.; Fuhr, O.; Brink, S.; Ruben, M. Spin Dynamics in the Negatively Charged Terbium (III) Bis-phthalocyaninato Complex. *J. Am. Chem. Soc.* **2009**, *131*, 4387–4396.

[128] Komijani, D.; Ghirri, A.; Bonizzoni, C.; Klyatskaya, S.; Moreno-Pineda, E.; Ruben, M.; Soncini, A.; Affronte, M.; Hill, S. Radical-lanthanide ferromagnetic interaction in a Tb^{III} bis-phthalocyaninato complex. *Phys. Rev. Materials* **2018**, *2*, 024405.

[129] Weltner, W. Jr. *Magnetic Atoms and Molecules;* Dover Publications, Inc.: New York, 1983.

[130] Brown, F. X.; Yamamoto, S.; Saito, S. The microwave spectrum of the HSiS radical in the 2A' ground electronic state. *J. Mol. Struct.* **1997**, *413-414*, 537–544.

[131] De Vore, T. C.; Weltner, W. Titanium difluoride and titanium trifluoride molecules: electron spin resonance spectra in rare-gas matrices at 4 K. *J. Am. Chem. Soc.* **1977**, *99*, 4700–4703.

[132] Knight, L. B. Jr.; Weltner, W. Jr. Hyperfine Interaction, Chemical Bonding, and Isotope Effect in ZnH, CdH, and HgH Molecules. *J. Chem. Phys.* **1971**, *55*, 2061–2070.

[133] Knight, L. B. Jr.; Fisher, T. A.; Wise, M. B. Photolytic codeposition generation of the HgF radical in an argon matrix at 12 K: An ESR investigation. *J. Chem. Phys.* **1981**, *74*, 6009–6013.

[134] Frisch, A.; Aikawa, K.; Mark, M.; Ferlaino, F.; Berseneva, E.; Kotochigova, S. Hyperfine structure of laser-cooling transitions in fermionic erbium-167. *Phys. Rev. A* **2013**, *88*, 032508.

[135] McConnell, H. M.; Chesnut, D. B. Theory of Isotropic Hyperfine Interactions in π-Electron Radicals. *J. Chem. Phys.* **1958**, *28*, 107–117.

[136] Pérez-Juste, I.; Carballeira, L. Theoretical study of the electronic structure of HXY/XYH radicals (X = C,Si;Y = O,S). *J. Chem. Phys.* **2007**, *127*, 164303.